The Eurasia Proceedings of Science, Technology, Engineering & Mathematics (EPSTEM)
ISSN: 2602-3199

The Eurasia Proceedings of Science, Technology, Engineering & Mathematics (EPSTEM), 2024

Volume 32, Pages 439-448

IConTES 2024: International Conference on Technology, Engineering and Science

Design and Numerical Investigation of Highly Photovoltaic Efficiency of Novel Non-Toxic Double Perovskite Solar Cell with Igzo as Electron Transport Layer

Abdelkrim El-Hasnaine Merad
Abou Bekr Belkaid University of Tlemcen

Souheyla Mamoun
Abou Bekr Belkaid University of Tlemcen

Abd-El-Illah Abbaci
Abou Bekr Belkaid University of Tlemcen

Abstract: The development of lead-free perovskite solar cells, is indeed a promising solution to the toxicity issue associated with traditional lead-based perovskites. These lead-free alternatives aim to maintain high efficiency while being environmentally friendly. In this context, we aim to propose a novel lead-free double perovskite solar cell with IGZO as electron transport layer (ETL). It has been demonstrated recently that this inorganic halide double perovskite with the structure A_2BX_6 is more stable compared to the lead-free perovskite with the structure ABX_3. We design our solar cell with the planar architecture where the perovskite layer is sandwiched between an electron transport layer IGZO and a hole transport layer $MoSe_2$. This contributes to efficient charge separation and collection, which is crucial for the performance of the solar cell. Our work focuses on the optimization and analysis of various key parameters governing perovskite solar cell performance, including the thicknesses of all layers, the acceptors N_A and defects N_t charge carrier densities, parasitic series resistance R_S and the working temperature T. The current-voltage characteristics (J-V), and quantum efficiency (QE) are analyzed via these key parameters. Our final optimal results, gives an impressive Power Conversion Efficiency (PCE) up to 25%. These findings represent a significant advancement and proposes the perovskite as a potential photoactive material in the renewable energy technology.

Keywords: Lead-free halide double perovskite solar cell, SCAPS simulation, IGZO, Acceptors density N_A, Defect density N_t, Series resistance R_S, Working temperature T.

Introduction

Recently, researchers have turned their attention to investigating the ABX_3 perovskite alternative structure known as inorganic halide double perovskites (IHDP) A_2BX_6 (A= K^+, Rb^+, Cs^+, B= Sn^{2+}, Pd^{2+}, Pt^{2+}, X= Cl^-, Br^-, I^-) (Tranka et al., 2018; Bartel et al., 2019). These IHDP structures are being studied for their strong covalency within the $[BX_6]^{2-}$ cluster, offering a potential solution to the stability challenges faced by conventional Pb-based perovskites (Nair et al., 2022). In fact, in addition to the toxicity problem, $APbX_3$ perovskites suffers from long-term instability caused by degradation after exposure to light, oxygen, moisture or heat, attributed to polymorphic transformation, hydration or decomposition. Both of these problems hamper their development and commercialization. (Ji et al., 2023).

Recently, Schwartz et al. (2020) synthesized a promising solar cell based on the IHDP Cs_2PtI_6 with excellent stability and oxidation resistance, high absorption coefficient ($4 \times 10^5\ cm^{-1}$ superior than $MAPbI_3$'one $10^5\ cm^{-1}$) and long carrier life time (superior than $2\ \mu s$ as long as that of $MAPbI_3$). The power conversion efficiency (PCE) of their adopted structure FTO/CdS/Cs_2PtI_6 ($10 - 15\ \mu m$)/ElectroDAG440B/Cu is about 10.7 % and can enhance to 13.88 % when ethylene diamine EDA (a chemical treatment) is added. This result

- Selection and peer-review under responsibility of the Organizing Committee of the Conference

makes Cs_2PtI_6 one of the most promising photovoltaic (PV) materials for such a first attempt. Furthermore, Yang et al. (2020) have confirmed the stability (experimentally and using ab initio calculation) of their synthesized IHDP Cs_2PtI_6 even when exposed to extreme condition such high humidity, high temperature and UV-light irradiation.

Using the one-dimensional solar cell simulator capacitance software SCAPS-1D (Burgelman et al., 2021). Cs_2PtI_6 was also theoretically studied by Shamna et al. (2022), AbdElaziz et al. (2022), Amjad et al. (2023). They showed that the PCE of their optimized structure FTO/ZnO/Cs_2PtI_6/MoO_3/C, FTO/WS_2/Cs_2PtI_6(0.4 μm)/Cu_2O/C and FTO/SnO_2/Cs_2PtI_6(0.4 μm)/MoO_3/C can reach $20.45\,\%$, $22.4\,\%$ and $23.52\,\%$ respectively.

In the ab initio papers of Cai et al. (2017) and Zhao et al. (2021). The co-workers have investigated the structural, electronic and optical properties of Cs_2PtI_6 and Rb_2PtI_6. Their results affirmed that Rb_2PtI_6 is stable (formation enthalpy equal to $-0.92\ eV/atom$), has suitable indirect band gap (1.3 eV **(**Cai et al., 2017). And 1.15 eV (Zhao et al., 2021). In the cubic structure) and high absorption in the photon energy range from 0 to $12\ eV$. Then, as Cs_2PtI_6, Rb_2PtI_6 can be highly desirable candidate, as lead-free double perovskite for photovoltaic (PV) applications.

In this context, we aim to investigate numerically, the photovoltaic (PV) performance of a new solar cell (SC) based on the IHDP Rb_2PtI_6. At the first step of our study, we try to constitute the experimental solar cell of Schwartz et al. (2020) based on Cs_2PtI_6 . We adopted their same architecture FTO/CdS/Cs_2PtI_6/Spiro-OMeTAD/C in the same conditions (at $T = 300K$, $f = 1\,MHz$, $R_s = 14\,\Omega\,cm^2$). Since we are arrived to reproduce their experimental PV performance, we are encouraged to study this SC replacing the cadmium sulfite CdS by another nontoxic ETL like Indium Gallium Zinc Oxyde IGZO and replacing the Spiro-OMeTAD by another non degradable inorganic ETL like molybdenum diselenide $MoSe_2$.

In order to enhance the power conversion efficiency of our novel Rb_2PtI_6 based solar cell (FTO/IGZO /Rb_2PtI_6/$MoSe_2$/C), we studied the effect of the absorber thickness, of its acceptors density N_A, of its defect density N_t, of series resistance (Rs), and of working Temperature T.

Devices Modeling and Simulation Parameters

We used SCAPS-1D code (Burgelman et al., 2021). Which is based theoretically on the fundamental equations: Poisson's equation (1) and continuity equation for holes and electrons equation (2):

$$\frac{d^2\psi}{dx^2} = \frac{e}{\varepsilon_0\varepsilon_r}\left[p(x) - n(x) + N_D - N_A + \rho_p - \rho_n\right] \tag{1}$$

Where ψ is electrostatic potential, n and p are electron and hole concentrations, ε_0 is vacuum and ε_r is relative permittivity, N_D and N_A are donor and acceptor doping density, ρ_n, ρ_p are electrons and holes distribution,

$$\frac{dJ_p}{dx} = \frac{dJ_n}{dx} = G - R \tag{2}$$

Where G is generation rate and R is recombination rate, J_p and J_n are holes and electron current densities.

Carrier transport occurs according to the following drift and diffusion equations:

$$J_n = \mu_n n \frac{d\varphi}{dx} + D_n \frac{dn}{dx} \tag{3}$$

$$J_p = \mu_p p \frac{d\varphi}{dx} + D_p \frac{dp}{dx} \tag{4}$$

The initial device architecture model FTO/ETL/A_2PtI_6/HTL/C is depicted in (Figure1.a). The cadmium sulfite CdS is used as an electron transport layer (ETL). The absorber or active layer is formed by the vacancy ordered double perovskite A_2PtI_6 material (where A=Cs/Rb). The 2,2'7,7'-tetrakis (N, N-di-p-methoxyphenyl-amin)-9,9'-spirobifluorene (Spiro-OMeTAD) is used as a hole transport layer (HTL). The Fluorine-doped tin oxide FTO is use in the front side and the carbon C is used as contact in the back side.

Our studied devices are a n-i-p type, for that, the n part is the ETL, the i part is the absorber A_2PtI_6 and the p part is the HTL. In order to make our model more realistic, we have considered the interface layers: interface 1 (ETL/A_2PtI_6) and interface 2 (A_2PtI_6/HTL), with a thickness of 5nm and keeping the same physical parameters as those of the perovskite.

Figure 1(c) illustrates the band gap alignment of HTL, ETL, and A_2PtI_6 with A=Cs/Rb, as well as the back and front device contacts of the initial and the alternative novel devices. The lowest unoccupied molecular orbital (LUMO) of IGZO (ETL) is in excellent alignment with the conduction band of Rb_2PtI_6. Likewise, the highest occupied molecular orbital (HOMO) of $MoSe_2$ (HTL) is well-aligned with the valence band level of an absorbing material.

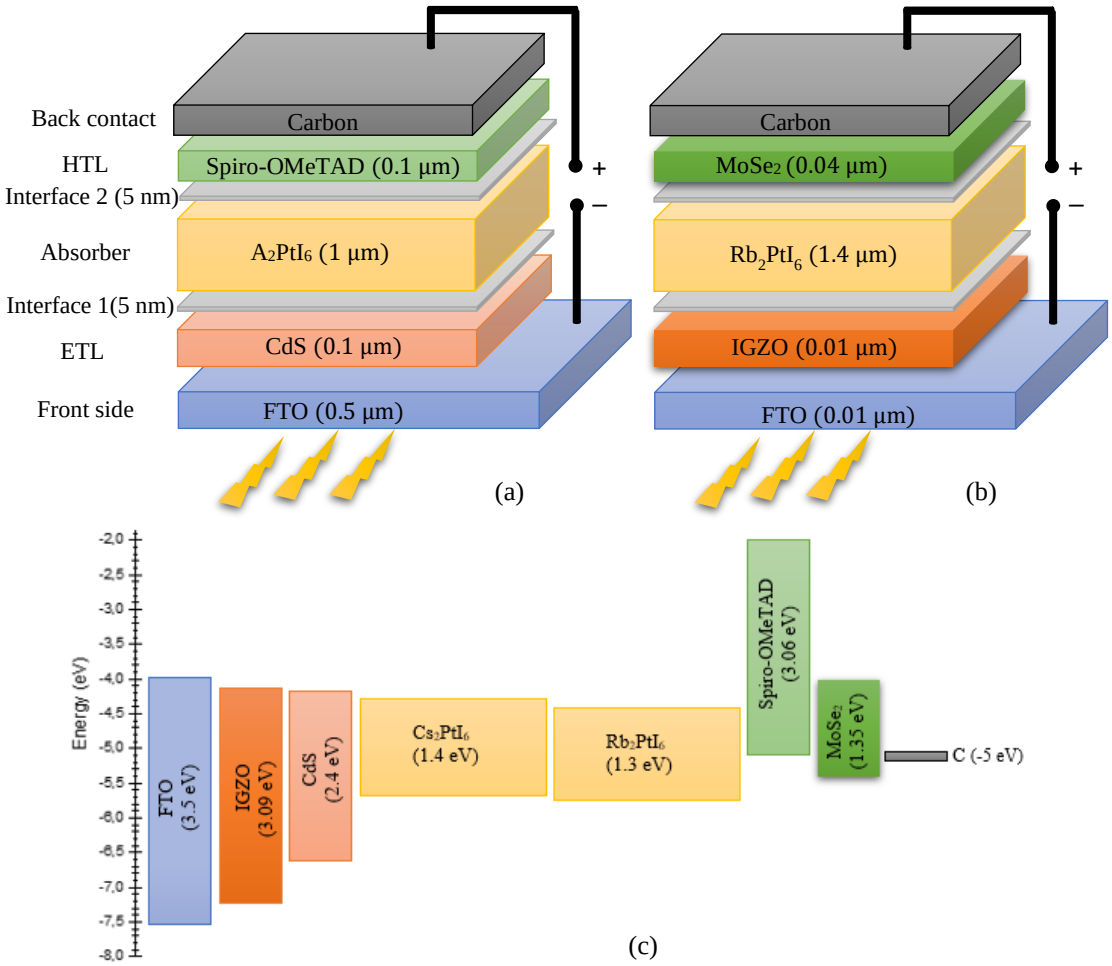

Figure 1. Architecture of (a) initial devices and (b) optimized device based on the platinum iodide perovskite where A=Cs/Rb. (c) Energy level diagram

To assess how the performance of PSCs is affected by operating temperature, we conducted simulations at approximately 300 K in an environment with an incoming power density of 100 mW/cm^2 and a frequency of 1 MHz. These simulations were conducted under the AM 1.5 G solar spectrum. We report in (Table 1**)** the input parameters for all HTL, ETL, A_2PtI_6 and FTO adopted for this study. Some of these parameters are derived from the literature and the others are obtained with our calculations since some parameters are not yet available in the literature for Rb_2PtI_6. For that, we have opted to the theoretical determination of such parameters based on the following equations:

$$N_t = \frac{1}{\sigma \tau V_{th}} \tag{5}$$

$$\mu_{n/p} = \frac{D_{n/p} q}{KT} \tag{6}$$

$$D_{n/p} = \frac{{l_{n/p}}^2}{\tau} \tag{7}$$

Where N_t is the defect density, μ is the electron and hole mobility, D is the diffusion coefficient, K is Boltzmann's constant, τ is the charge carrier lifetime, $l_{n/p}$ is the electron/hole diffusion length; σ is the capture cross-section of electron/hole and V_{th} is the thermal velocity of electron/hole. Also, the absorber layer effective conduction band density of states, N_c and effective valence band density of states, N_v are determined using the two following expressions:

$$N_c = 2\left(\frac{2\pi m_n^* KT}{h^2}\right)^{\frac{3}{2}} \quad \text{and} \quad N_v = 2\left(\frac{2\pi m_p^* KT}{h^2}\right)^{\frac{3}{2}} \tag{8}$$

Where m_n^* and m_p^* are the effective masses of electrons and holes, respectively.

Table 1. The input parameters of the adopted devices collected from our calculation and available data

	HTL		Absorber		ETL		Front side
Input parameter	Spiro-OMeTAD	$MoSe_2$	Cs_2PtI_6	Rb_2PtI_6	CdS	IGZO	FTO
Band gap, E_g (eV)	3.06 [a]	1.35 [b]	1.4 [c]	1.3 [f]	2.4 [i]	3.05 [b]	3.5 [a]
Affinity, χ (eV)	2.05 [a]	4.05 [b]	4.44 [d]	4.43 [d]	4.2 [i]	4.16 [b]	4 [a]
Relative Dielectric permittivity, ε_r	3 [a]	11.9 [b]	4.8 [e]	4.34 [g]	10 [i]	10 [b]	9 [a]
CB effective density of states, N_c (cm^{-3})	2.8×10^{19} [a]	2.8×10^{19} [b]	9×10^{18} [d]	7.5×10^{18} [d]	2.2×10^{18} [i]	5×10^{18} [b]	9.2×10^{18} [a]
VB effective density of states, N_v (cm^{-3})	10^{19} [a]	2.65×10^{19} [b]	4×10^{19} [d]	3.5×10^{19} [d]	1.8×10^{19} [i]	5×10^{19} [b]	1.8×10^{19} [a]
Electron mobility, $\mu_n(cm^2V^{-1}s^{-1})$	10^{-4} [a]	1450 [b]	0.19 [d]	0.65 [h]	100 [i]	15 [b]	20 [a]
hole mobility, $\mu_p(cm^2V^{-1}s^{-1})$	2×10^{-4} [a]	50 [b]	62.6 [c]	3.25 [h]	25 [i]	0.1 [b]	10 [a]
Electron effective mass, m_n^*	-	-	0.51 [f]	0.45 [f]	-	-	-
hole effective mass, m_p^*	-	-	1.45 [f]	1.245 [f]	-	-	-
Density of n-type doping, N_D (cm^{-3})	0	0	0	0	10^{18} [i]	10^{18} [b]	10^{19} [a]
Density of p-type doping, $N_A(cm^{-3})$	10^{18} [a]	4×10^{18} [b]	10^{15} [d]	10^{15} [d]	0	0	0
Density of defect, $N_t(cm^{-3})$	10^{14} [a]	10^{14} [b]	2.5×10^{12} [d]	3.5×10^{13} [d]	10^{19} [i]	10^{15} [b]	10^{15} [a]

[a] data from Jahantigh et al. (2019)
[b] data from Teyou Ngoupo et al. (2022)
[c] experimental data from Schwartz et al. (2020)
[d] our calculation
[e] experimental data from Yang et al. (2020)
[f] ab initio data from Cai et al. (2017)
[g] ab initio data from Zhao et al. (2021)
[h] from Yang et al. (2019)
[i] from Nykyry et al. (2019)

Results and Discussion

Verification of the Devices Model

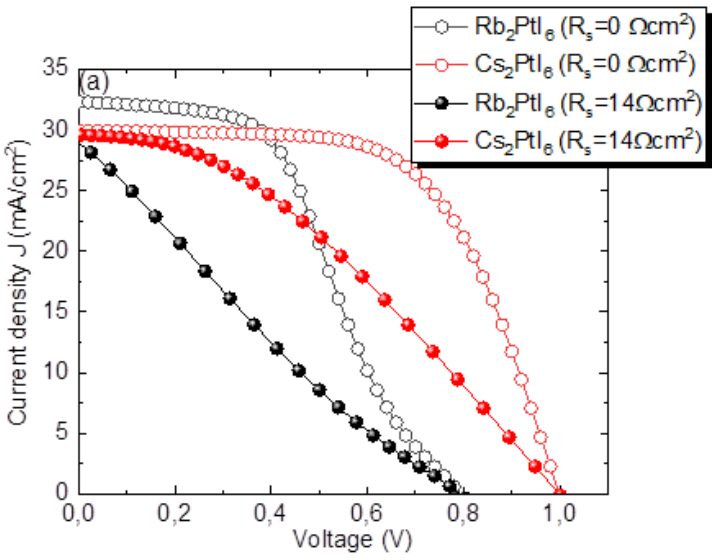

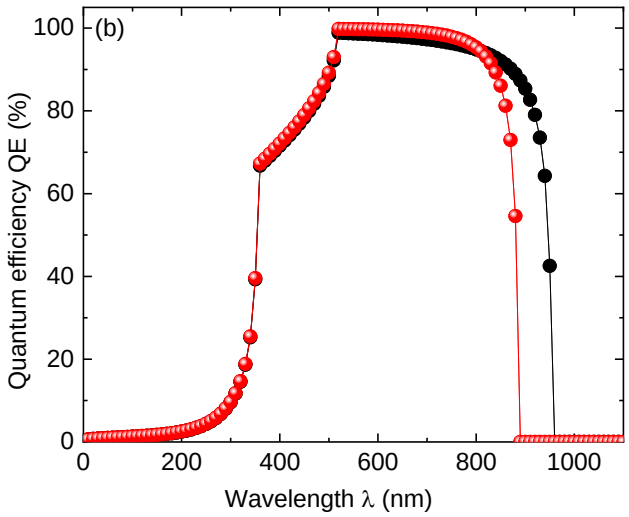

Figure 2. Initial PV simulation results of Cs_2PtI_6 and Rb_2PtI_6 based solar cells for ($R_s = 0$ and $R_s = 14\ \Omega\ cm^2$) (a) J-V curves (b) QE versus wavelength

The initial PV simulation of FTO/CdS/A_2PtI_6/Spiro-OmeTAD/C with A=Cs/Rb based solar cells is conducted for ($R_s = 0$ and $R_s = 14\ \Omega\ cm^2$). Figure 2 illustrates the photovoltaic characteristics, such as the current density curves (J-V curves) and the quantum efficiency (QE). Our obtained PV values of FTO/CdS/Cs_2PtI_6/Spiro-OmeTAD/C solar cell (Figure 1.a) align with experimental outcomes reported by (Schwartz et al., 2020). (Table 2) thereby reinforcing the integrity of the numerical simulation. As a result, the chosen material parameters for the device model are justified. As a second step, we have taken our novel solar cell model (FTO/IGZO/Rb_2PtI_6/$MoSe_2$/C) and proceeded our optimization by varying the thicknesses of all constructing layers. The optimized solar cell based on the platinum iodide perovskite with the optimal thicknesses is depicted in Figure 1.b.

Table 2. J-V characteristic of initial Rb_2PtI_6 and Cs_2PtI_6 based solar cells compared with other simulation and experimental available results for ($\boldsymbol{R_s = 0}$ **and** $\boldsymbol{R_s = 14\ \Omega\ cm^2}$)

Structure	R_s ($\Omega\ cm^2$)	V_{oc} (V)	J_{sc} (mA/cm^2)	FF (%)	PCE (%)
FTO ($0.5\mu m$)/CdS ($0.1\mu m$)/ Rb_2PtI_6 ($1\mu m$)/Spiro-OmeTAD ($0.1\mu m$)/C	0	0.79	32.33	46.15	11.83
FTO ($0.5\mu m$)/CdS ($0.1\mu m$)/ Rb_2PtI_6 ($1\mu m$)/Spiro-OmeTAD ($0.1\mu m$)/C	14	0.79	28.95	22.23	5.10
FTO ($0.5\mu m$)/CdS ($0.1\mu m$)/ Cs_2PtI_6 ($1\mu m$)/Spiro-OmeTAD ($0.1\mu m$)/C	0	0.99	29.95	61.69	18.45
FTO ($0.5\mu m$)/CdS ($0.1\mu m$)/ Cs_2PtI_6 ($1\mu m$)/Spiro-OmeTAD ($0.1\mu m$)/C	14	0.99	29.60	36.19	10.70
FTO/CdS (0.08-$0.1\mu m$)/ Cs_2PtI_6 (10-$15\mu m$)/ElectroDAG 440B/Cu	14	0.9 [a]	19.83 [a]	59.85 [a]	10.70 [a]
FTO/CdS/ Cs_2PtI_6/Spiro-OmeTAD/C	14	1.12 [b]	20.1 [b]	44 [b]	10.16 [b]

[a]: Experimental results from Schwartz et al. (2020)
[b]: SCAPS-1D simulation results (Abdelaziz et al. 2023)

Absorber Acceptor Density N_A Effect

The enhancement of the photovoltaic performance of a solar cell depends crucially on the optimization of the absorber layer thickness as well as the acceptor doping density N_A. To illustrate this effect, we have shown in (Figure 3) the contour plot of the photovoltaic parameters as function of absorber thickness and N_A of our simulation for absorber thickness varying from 0.2 to 1.4 μm and N_A varying from 10^{15} to 10^{20} cm^{-3}. The figure reveals that the highest PCE value is 23.75% for high thickness and high N_A. it is evident that lower absorber thickness leads to lower PCE. This is because for thin absorber layers, most incident photons are transmitted through the material, leading to reduced generation of electron-hole (e-h) pairs and consequently, lower PCE. However, increasing the absorber thickness leads to an increase in optical absorption and generation of (e-h) pairs, which results in an improvement in PCE.

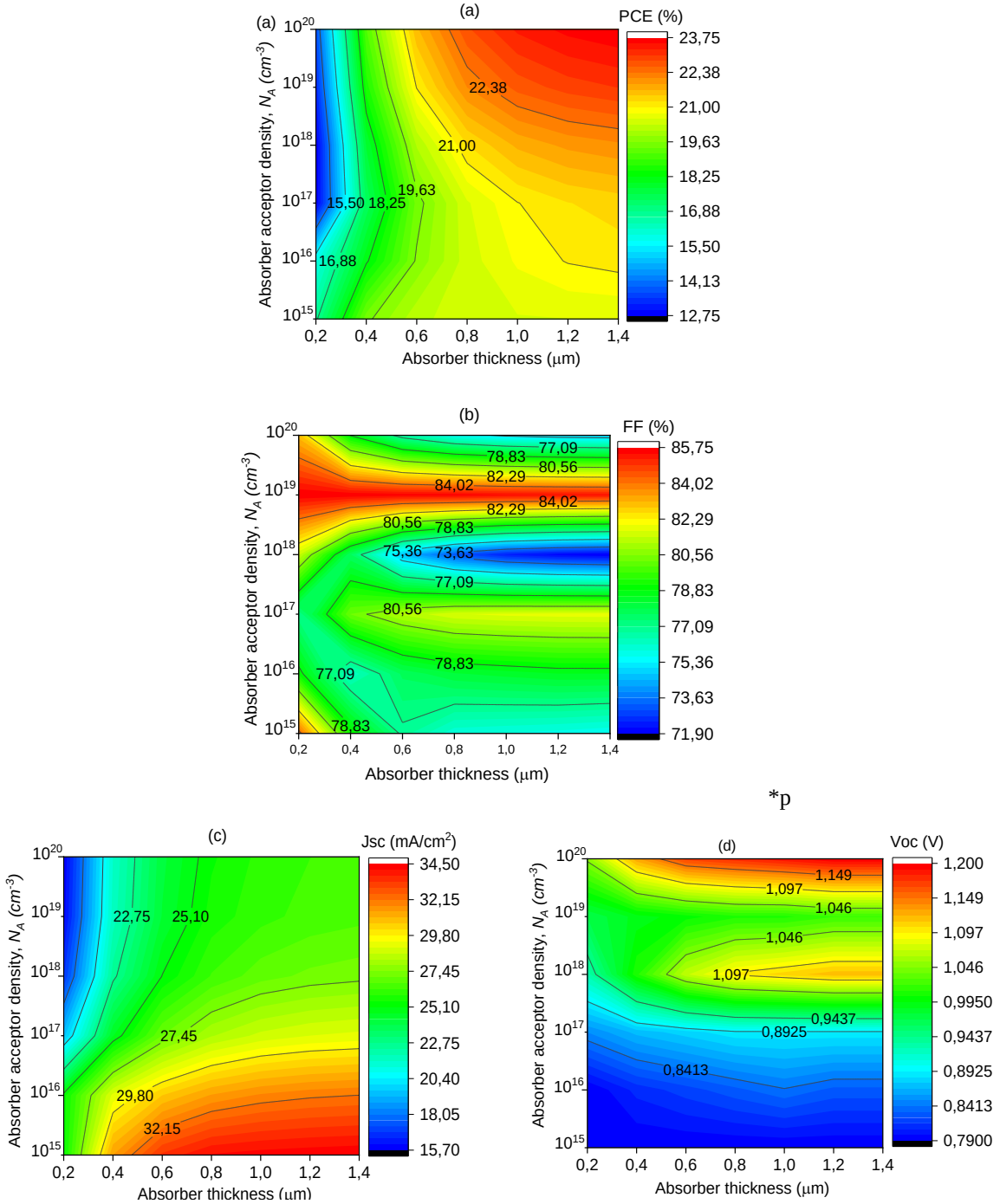

*p

Figure 3. Contour plot of photovoltaic parameters as function of absorber thickness and N_A.

Absorber Defect Density N_t Effect

The impact of the absorber defect density on the photovoltaic parameters of the PSC is illustrated in (Figure 4) by a contour plot. As the defect density (or trap density) increases in the absorber material for higher thickness, Jsc remains constant between 10^{10} cm^{-3} and 10^{11} cm^{-3} and after that, it shows a gradual decrease up to 10^{14} cm^{-3}. This decrease occurs because the traps tend to trap charge carriers, preventing them from participating in the current flow in the solar cell. The Voc decreases as the defect density increases. This phenomenon occurs because the defects in the perovskite material serve as sites where electrons and holes recombine. This recombination process decreases the amount of charge carriers available for collection by the solar cell, thus reducing both the voltage and output current. The increased defect density facilitates the recombination of electrons and holes, hampering their ability to generate current efficiently and leading to a decrease in Voc.

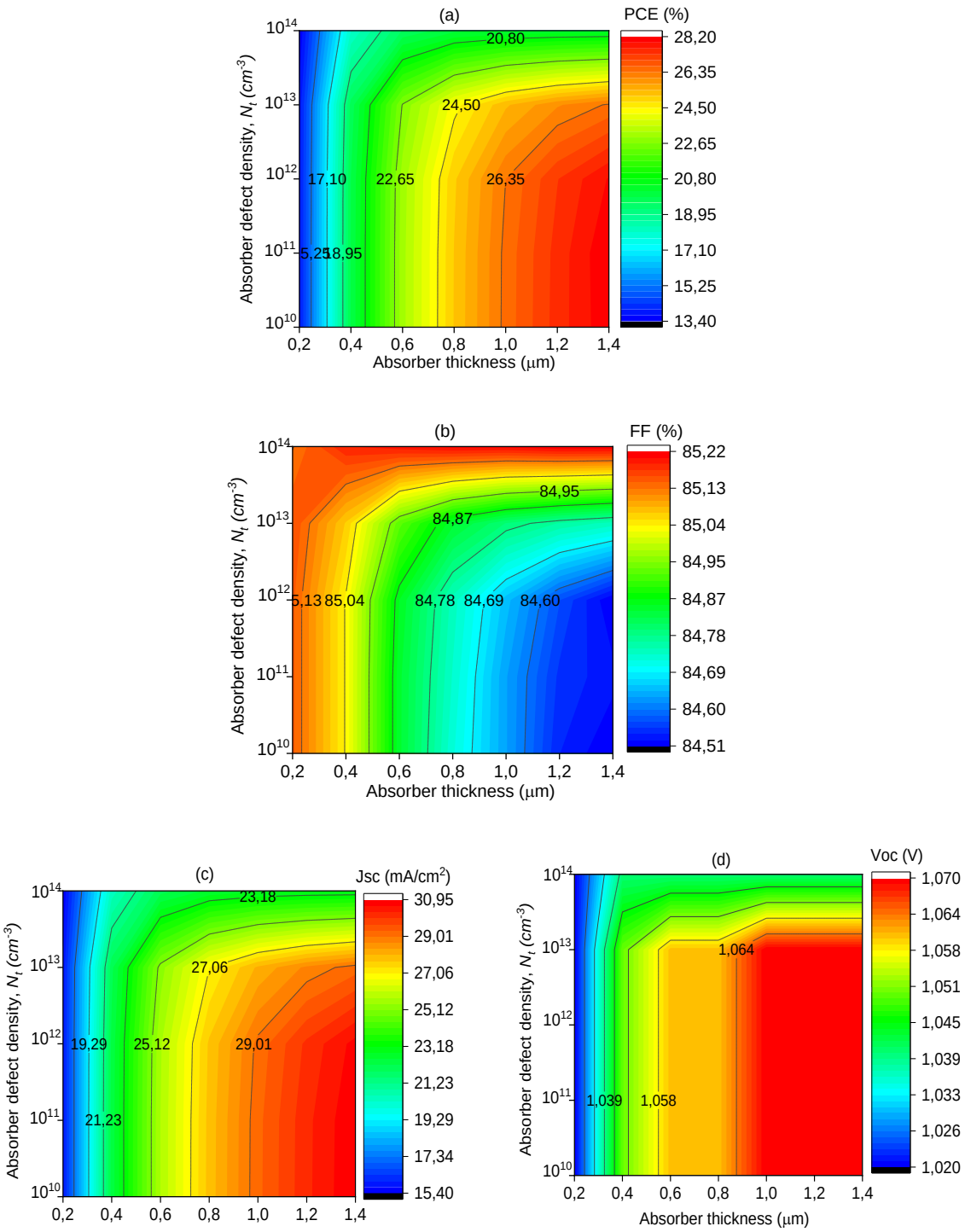

Figure 4. Contour plot of photovoltaic parameters as function of absorber thickness and N_t.

Series Resistance R_S Effect

The optimum performance of a solar cell corresponds to the ideal value of R_S which is equal to zero, but in practical reality, this is not the case for R_S. In fact, the series resistance is due to factors such as ohmic contacts, metallic contacts, ITO sheet resistance, contact resistance inside the cell and manufacturing imperfections. Figure 5 shows the impact of R_S on various photovoltaic parameters of PSC including PCE, Voc, Jsc and FF. As R_S increases, PCE decreases significantly, from 28.14% to 16.7%, while the Voc and Jsc parameters remain practically constant.

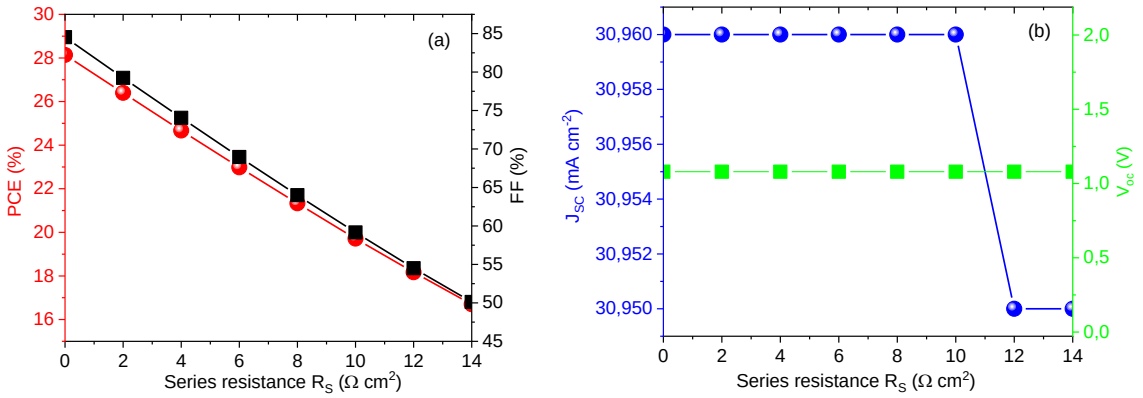

Figure 5. Series resistance effect on the photovoltaic parameters.

Working Temperature Effect

One of major problems for PSCs is their degradation over time under exposure to high temperatures due to the chemical and structural changes of perovskite materials at elevated temperatures. This can negatively impact their performance. Indeed, the interfaces between different layers in the solar cell can be affected by temperature, leading to increased recombination and reduced charge transport. Hence, to examine the behavior of PSCs in a real-world setting, a performance study across a temperature range spanning from 270 K to 370 K is conducted.

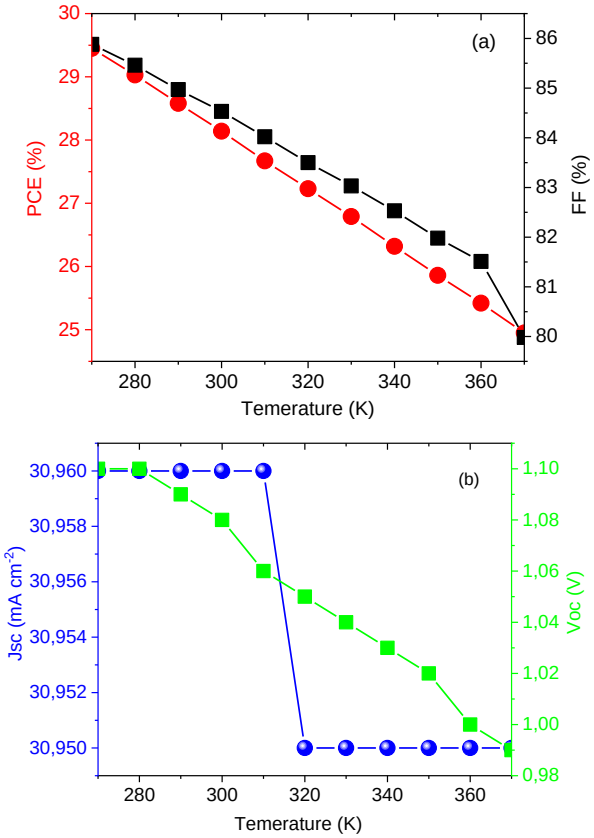

Figure 6. Temperature effect on the photovoltaic parameters.

Figure 6 illustrates this effect. A constant decrease in PCE, Voc and FF values as the temperature increases, while the Jsc remains stable up to 310 K and shows a smaller decrease up to 320 K and after that it continues its stability up to 370 K.

Conclusion

This work provides a valuable design of the planar architecture of the solar cell where the double perovskite layer is sandwiched between an electron transport layer IGZO and a hole transport layer $MoSe_2$. We have optimized and analyzed of various fundamental parameters governing perovskite solar cell performance, including the thicknesses of all layers, the acceptors N_A and defects N_t charge carrier densities, parasitic series resistance Rs and the working temperature T. The current-voltage characteristics (J-V), and quantum efficiency (QE) are analyzed via these key parameters. Our final optimal results, gives an impressive power conversion efficiency (PCE) up to 28.14% for $N_A=10^{20}$ cm^{-3} and $N_t=10^{10}$ cm^{-3}. These predictive findings propose our novel lead-free double perovskite solar cell as a potential candidate for non-toxic an environmentally friendly solar cell applications.

Scientific Ethics Declaration

The authors declare that the scientific ethical and legal responsibility of this article published in EPSTEM Journal belongs to the authors.

Acknowledgements

The authors are thankful to Professor Marc Burgelman and his coworkers at the University of Ghent, Belgium, for providing the SCAPS-1D software used in this study.

Notes

* This article was presented as an oral presentation at the International Conference on Technology, Engineering and Science (www.icontes.net) held in Antalya/Turkey on November 14-17, 2024.

References

AbdElAziz, H. H., Taha, M., El Rouby, W.M.A., Khedr, M.H., & Saad, L. (2022). Evaluating the performance of $Cs_2PtI_{6-x}Br_x$ for photovoltaic and photocatalytic applications using first-principles study and SCAPS-1D simulation. *Heliyon, 8*(10), e10808.

Amjad, A., Qamar, S., Zhao, C., Fatima, K., Sultan, M., & Akhter, Z. (2023). Numerical simulation of lead-free vacancy ordered Cs_2PtI_6 based perovskite solar cell using SCAPS-1D. *RSC Advances,13*(33), 23211–23222.

Bartel, C.J., Sutton, C., Goldsmith, B.R., Runhai, O., Musgrave, C.B., Ghiringhelli, L.M., & Scheffler, M. (2019). New tolerance factor to predict the stability of perovskite oxides and halides. *Science Advances, 5(2),* eaav0693.

Burgelman, M., Decock, K., Niemegeers, A., Verschraegen, J., & Degrave, S. J. F. (2021). *SCAPS manual.* Retrieved from https://scaps.elis.ugent.be/SCAPS%20manual%20most%20recent.pdf

Cai, Y., Xie, W., Ding, H., Chen, Y., Thirumal, K., Wong, L.H., Mathews, N., Mhaisalkar, S.G., Sherburne, M., & Asta, M. (2017). Computational study of halide perovskite-derived a_2bx_6 inorganic compounds: chemical trends in electronic structure and structural stability. *Chemistry of Materials, 29*(18), 7740−7749.

Jahantigh, F., & Safikhani, M. J. (2019). The effect of HTM on the performance of solid-state dye-sanitized solar cells (SDSSCs): A SCAPS-1D simulation study. *Applied Physics A, 125*(4), 276.

Ji, F., Boschloo, G., Wang, F., & Gao, F. (2023). Challenges and progress in lead-free halide double perovskite solar cells. *Solar RRL, 7*(6), 2201112.

Nair, S. S., Krishnia, L., Trukhanov, A., Thakur P., & Thakur A. (2022). Prospect of double perovskite over conventional perovskite in photovoltaic applications. *Ceramics International, 48*(23), 34128.

Nykyruy, L.I., Yavorskyi, R.S., Zapukhlyak, Z.R., Wisz, G., & Potera, P. (2019). Evaluation of CdS/CdTe thin film solar cells: SCAPS thickness simulation and analysis of optical properties. *Optical Materials* 92, 319-329.

Schwartz, D., Murshed, R., Larson, H., Usprung, B., Soltanmohamad, S., Pandey, R., Barnard, E.S., Rockett, A., Hartmann, T., Castelli, I.E., & Bansal S. (2020). Air stable, high-efficiency, pt-based halide perovskite solar cells with long carrier lifetimes. *Physica Statu Solidi, 14*, 2000182.

Shamna, M.S. & Sudheer, K.S. (2022). Device modeling of Cs_2PtI_6-based perovskite solar cell with diverse transport materials and contact metal electrodes: A comprehensive simulation study using solar cell capacitance simulator. *Journal of Photonics for Energy, 12,* 032211.

Tanaka, H., Oku, T., & Ueoka, N. (2018). Structural stabilities of organic–inorganic perovskite crystals. *Japanese Journal of Applied Physics, 57*(8S3), 08RE12.

Teyou- Ngoupo, A., & Ndjaka, J.M.B. (2022). Performance enhancement of Sb_2Se_3 -based solar cell with hybrid buffer layer and $MoSe_2$ as a hole transport material using simulator device. *Discover Mechanical Engineering, 1*(1), 5.

Yang, S., Wang, L., Zhao, S., Liu, A., Zhou, Y., Han, Q., Yu, F., Gao, L., Zhang, C., & Ma, T. (2020). A novel lead-free material Cs_2PtI_6 with narrow bandgap and ultra-stable for its photovoltaic application. *ACS Appl. Mater. Interfaces, 12*(40), 44700–44709.

Yang, Z., Yu, Z., Wei, H., Xiao, X., Ni, Z., Chen, B., ... & Huang, J. (2019). Enhancing electron diffusion length in narrow-bandgap perovskites for efficient monolithic perovskite tandem solar cells. *Nature Communications, 10*(1), 4498.

Zhao, X.H., Wei, X.N., Tang, T.Y., Gao, L.K., Xie, Q., Lu, L.M. & Tang, Y.L. (2021). First-principles study on the structural, electronic and optical properties of vacancy-ordered double perovskites Cs_2PtI_6 and Rb_2PtI_6. *Optical Materials 114,* 110952.

Author Information

Abdelkrim El-Hasnaine Merad
Solid State Physics Team, Theoretical Physics Laboratory, Faculty of Sciences, A Belkaid University, Box 119, 13000, Tlemcen, Algeria
Contact e-mail: abdelkrim.merad@univ-tlemcen.dz

Souheyla Mamoun
Solid State Physics Team, Theoretical Physics Laboratory, Faculty of Sciences, A Belkaid University, Box 119, 13000, Tlemcen, Algeria

Abd-El-Illah Abbaci
Solid State Physics Team, Theoretical Physics Laboratory, Faculty of Sciences, A Belkaid University, Box 119, 13000, Tlemcen, Algeria

To cite this article:

Merad, A.E., Mamoun, S., & Abbaci A.E. (2024). Design and numerical investigation of highly photovoltaic efficiency of novel non-toxic double perovskite solar cell with IGZO as electron transport layer. *The Eurasia Proceedings of Science, Technology, Engineering & Mathematics (EPSTEM), 32,* 439-448.